57. On the Mechanism of Magnetic Quenching of Fluorescence in Gaseous State

by **A. Matsuzaki** and **S. Nagakura**

Research Institute of Physical and Chemical Research, Wako, Saitama, Japan

In Memoriam Prof. *Heinrich Labhart*

(6.XII.77)

Summary

The pressure dependence of fluorescence quenching of gaseous glyoxal has been measured in the presence of a magnetic field of 1–8 kG. Below 5 kG both the collision free lifetime and the collisional quenching constant were found to be dependent upon magnetic field strength. Above 5 kG the collisional quenching constant turned out to be nearly equal to the value without magnetic field and the collision free lifetime took a constant value larger than that without magnetic field.

The magnetic enhancement of the intramolecular radiationless transition of gaseous molecules has been studied theoretically. The phenomenon is shown to be explained by considering two mechanisms, mechanisms I and II. Mechanism I is due to the interaction of a primary state with secondary states through the *Zeeman* hamiltonian. Mechanism II is due to the shift and broadening of appropriate rovibronic levels by the *Zeeman* effect.

Introduction. – Magnetic field effects upon emission from molecules in the gaseous state have been observed with iodine [1–7], nitrogen dioxide [8] [9], carbon disulfide [10], and glyoxal [11]. The magnetic quenching of luminescence observed with the iodine molecule was interpreted in terms of a field induced predissociation. In 1932 *van Vleck* [3] pointed out that the transition from the $^3\Pi_{0_u^+}$ state to the dissociative $^3\Pi_{0_u^-}$ state was induced in the presence of a magnetic field. *Solarz et al.* [8] [9] found that the fluorescence from the $^2B_2$ state of nitrogen dioxide is quenched in the presence of a magnetic field. In this case, intramolecular and intermolecular processes are both affected by a magnetic field. In iodine and nitrogen dioxide the quenched states are the magnetic states, the triplet state in iodine and the doublet state in nitrogen dioxide.

Recently, the present authors found the magnetic quenching of fluorescence from excited singlet states: the $^1A_2$ state of carbon disulfide [10] and the ^1A_u state of glyoxal [11]. In these cases, intramolecular nonradiative processes were found to be enhanced in the presence of a magnetic field. Furthermore, according to our experimental result of carbon disulfide, the magnetic field dependence of $(\tau_0/\tau)-1$ (τ_0 and τ are the fluorescence lifetimes without and with magnetic field,

respectively) consists of the two components: the low-field component increasing rapidly with increasing magnetic field below 4 kG and the high-field component proportional to the square of the magnetic field in the range higher than 5 kG *(Fig. 1)*. In the case of glyoxal, the $(\tau_0/\tau)-1$ value is saturated at ~700 G and the higher magnetic field component is not observed. These facts indicate that the magnetic quenching of fluorescence is due to the combination of two different mechanisms. *Atkins & Stannard* [12] presented a theory for the magnetic quenching of fluorescence introducing the direct and indirect mechanisms.

Very recently, *Küttner et al.* [13] observed fluorescence quenching of gaseous glyoxal at various pressures with different collision partners as a function of the magnetic field below 2 kG. They found that the magnetic quenching was only observed in the presence of collision and the collision-free lifetime was unaffected by a magnetic field near 1 kG, although the magnetic field enhanced intersystem crossing. Previously, we found that the magnetic quenching of the fluorescence of glyoxal occurred through the change of the collision-free lifetime in the presence of a magnetic field of 5 kG and was due to the enhancement of intersystem crossing [11]. From the comparison of our result at 5 kG with that of *Küttner et al.* at 1 kG, we expected that at the higher magnetic field, the magnetic field effect upon the intramolecular process might become explicitly observable because of a shift and diffusing of energy – acceptable (secondary) rovibronic levels, while at the lower magnetic field their densities might be sparse and the energy decay might occur only through collisions. To verify this expectation, in the present study we have measured magnetic field effects on the collisional quenching constant and collision-free lifetime of the fluorescence of glyoxal changing magnetic field strength more widely (0–8.04 kG) than in the previous study [11]. The result fulfills our expectation.

According to the indirect mechanism by *Atkins & Stannard* [12] a magnetic field enhances radiationless decay of a primary state into a quasi-continuum through the mixing with another discrete state. The above-mentioned facts suggest the necessity to modify the mechanism to some extent. In the present paper we propose mechanism I and mechanism II for the magnetic quenching of fluorescence in the gaseous state. Mechanism I is similar to the direct mechanism by *Atkins & Stannard*. Mechanism II is the enhancement of mixing of a primary state with

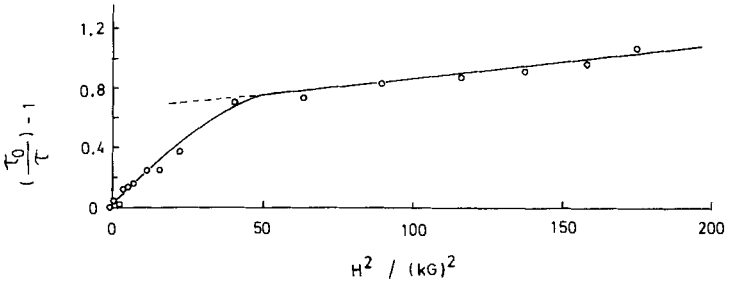

Fig. 1. *Plots of* $(\tau_0/\tau - 1)$ *versus the square of magnetic field strength* $(\mathscr{H}^2)$ *for* CS_2 (the pressure of CS_2 is 10^{-3} Torr)

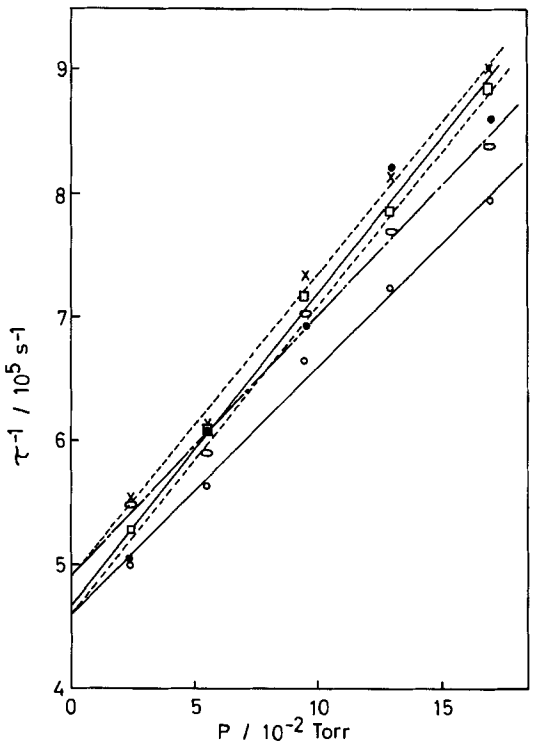

Fig. 2. *Plots of the decay rate of fluorescence from the* $^1A_u(0)$ *state versus glyoxal pressure (P)*
——○—— in the absence of a magnetic field
----●---- in the presence of a magnetic field of 1.02 kG; ——□—— 1.99 kG; ----x---- 3.92 kG; -·- o -·- 8.04 kG

secondary states through such well-known interactions as vibronic and spin-orbit couplings: the magnetic field decreases the energy separation between them by the *Zeeman* effect and enhances the couplings. Quite recently, the selection rule for mechanism I was studied independently by *Stannard* [14] and by the present authors [15]. We report the application of the rule to carbon disulfide, glyoxal, and iodine.

Collision-Free Lifetimes and Collisional Quenching Constants of Glyoxal. – Lifetimes of fluorescence from the $^1A_u(0)$ state of gaseous glyoxal under various pressures were observed in the presence of a magnetic field of 0, 1.02, 1.99, 3.92, and 8.04 kG. The $1/\tau$ values are plotted against glyoxal pressures in *Figure 2*. From the slopes and the intercepts with the ordinate of straight lines in *Figure 2*, the collisional quenching constants, k, and the collision-free lifetimes, τ_0, are obtained for the respective field strengths. The k and $1/\tau_0$ values are plotted as a function of field strength $\mathscr{H}$. The results are shown in *Figure 3*. The k value increases with increasing field strength at low field, but decreases at the fields higher than 2 kG. The value at 8.04 kG is nearly equal to the value without the magnetic field. The $1/\tau_0$ value increases with increasing field strength below 5 kG and is saturated to a

constant value of $4.9\times 10^5\ s^{-1}$ at ~ 5 kG. This shows that at higher magnetic fields the magnetic quenching of the fluorescence of glyoxal due to enhancement of intramolecular processes turns out to be explicitly observable because of the increase in the state density of a secondary state due to the broadening of its rovibronic levels and also due to coupling with the higher rovibronic levels of the ground state, while at lower fields the level density of the secondary state is sparse and the energy is lost through collision. It may be noticed, however, that a magnetic field enhances intramolecular nonradiative processes even at low field strength, as was pointed out by *Küttner et al.* [13].

Mechanism of Magnetic Quenching. – We consider the two types of mechanisms for the magnetic enhancement of intramolecular nonradiative process from a primary state, ψ_p to secondary states, ψ_s; mechanism I and mechanism II.

Mechanism I. Mechanism I is due to the coupling of a primary state with quasi-continuum secondary states, particularly with the higher rovibronic levels of the ground state, by the *Zeeman* hamiltonian $\mathscr{H}_z$. The nonradiative decay constant for this case is represented by the following equation [16] [17].

$$\begin{aligned} k_{nr} &= 2\pi\hbar\rho\,|\langle\psi_p|\mathscr{H}_{vib}+\mathscr{H}_{so}+\mathscr{H}_z|\psi_s\rangle|^2 \\ &= 2\pi\hbar\rho\,[\,|\langle\psi_p|\mathscr{H}_{vib}+\mathscr{H}_{so}|\psi_s\rangle|^2 \quad +\langle\psi_p|\mathscr{H}_{vib}+\mathscr{H}_{so}|\psi_s\rangle\langle\psi_p|\mathscr{H}_z|\psi_s\rangle \\ &\quad +\langle\psi_p|\mathscr{H}_z|\psi_s\rangle\langle\psi_p|\mathscr{H}_{vib}+\mathscr{H}_{so}|\psi_s\rangle \quad +|\langle\psi_p|\mathscr{H}_z|\psi_s\rangle|^2] \\ &= k_0+k_{mag}(\mathscr{H})+k_{mag}(\mathscr{H}^2) \\ &= k_0+k_{mag} \end{aligned} \tag{1}$$

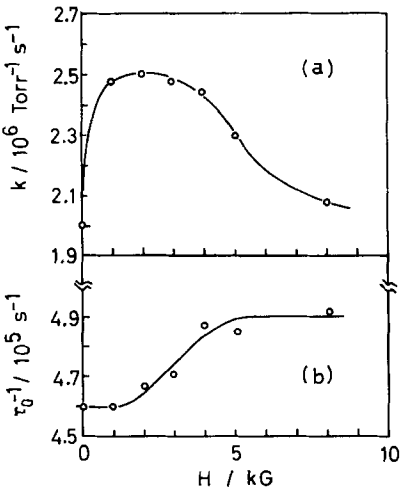

Fig. 3. (a) *Plots of the collisional quenching constant of the* $^1A_u(0)$ *state* (k) *versus the magnetic field strength* ($\mathscr{H}$)
(b) *Plots of the inverse of the collision-free lifetime of the* $^1A_u(0)$ *state* (τ_0^{-1}) *versus the magnetic field strength* ($\mathscr{H}$)

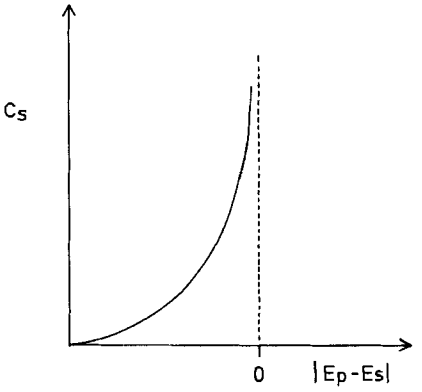

Fig. 4. *The dependence of* c_s *on the energy separation* $|E_p - E_s|$

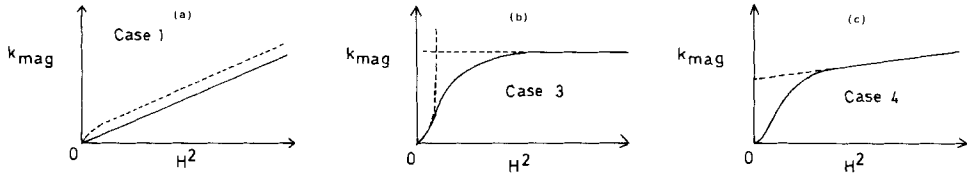

Fig. 5. *The dependence of magnetic quenching constant* k_{mag} *on the square of a magnetic field strength* $\mathscr{H}^2$
(a) for case 1; —— for the case of $\langle \psi_p | \mathscr{H}_{so} + \mathscr{H}_{vib} | \psi_s \rangle = 0$; ---- for the case of $\langle \psi_p | \mathscr{H}_{so} + \mathscr{H}_{vib} | \psi_s \rangle \neq 0$: (b) for case 3: (c) for case 4

Here $\mathscr{H}_{vib}$ and $\mathscr{H}_{so}$ are the hamiltonians of vibronic and spin-orbit couplings, respectively.

The plot of k_{mag} versus the square of magnetic field strength $\mathscr{H}^2$ is shown in *Figure 5a*. When the matrix element $\langle \psi_p | \mathscr{H}_{vib} + \mathscr{H}_{so} | \psi_s \rangle$ is zero, k_{mag} is equal to $k_{mag}(\mathscr{H}^2)$ and the plot of k_{mag} versus $\mathscr{H}^2$ gives a straight line. The selection rule for this mechanism is discussed in a later part of this paper.

Mechanism II. Mechanism II is based on the shift of the rovibronic levels belonging to secondary states by the *Zeeman* effect. This mechanism becomes effective in the case where the level densities of the secondary states are sparse at zero magnetic field. When the level densities of secondary states are sparse to some extent, a wavefunction of a primary state is represented by eq. (2).

$$\psi_p' = c_p \psi_p + \sum_s \frac{\langle \psi_s | \mathscr{H}_{vib} + \mathscr{H}_{so} | \psi_p \rangle}{E_p - E_s} \psi_s \qquad = c_p \psi_p + \sum_s c_s \psi_s \tag{2}$$

The decay constant of a primary state into secondary states is proportional to $\sum_s c_s^2$. The rovibronic levels of the secondary states are shifted or broadened by the *Zeeman* effect, and come close to those of the primary state: that is, the energy difference $|E_p - E_s|$ in eq. (2) decreases and c_s^2 increases rapidly with increasing magnetic field, as is shown in *Figure 4*. When the rovibronic levels are broadened and become diffuse at high field[1]), the magnetic field effect on c_s may be saturated. Therefore, in mechanism II, k_{mag} increases rapidly with increasing field strength at low magnetic fields, and is saturated at high fields, as is shown in *Figure 5b*.

We can classify the magnetic quenching of fluorescence of excited molecule in gas phase into the following four cases.

Case 1. When secondary states are a quasi-continuum and $\langle \psi_p | \mathscr{H}_z | \psi_s \rangle$ is nonzero, the magnetic quenching occurs by mechanism I. A magnetic quenching constant k_{mag} varies with $\mathscr{H}$ as is shown in *Figure 5a*. The magnetic quenching in the $^3\Pi_{0u}^+$ state of the iodine molecule belongs to this case.

Case 2. When secondary states are a quasi-continuum and $\langle \psi_p | \mathscr{H}_z | \psi_s \rangle$ is zero, the magnetic quenching is not observed.

Case 3. When secondary states are sparse and $\langle \psi_p | \mathscr{H}_z | \psi_s \rangle$ is zero, the magnetic quenching occurs by mechanism II. k_{mag} varies with $\mathscr{H}$ as is shown in

---

[1]) The broadening and diffusing of rovibronic levels by the *Zeeman* effect were observed with the absorption spectrum of gaseous sulfur dioxide [18].

Figure 5b. The magnetic quenching in the ^1A_u state of glyoxal is an example of this case.

Case 4. When secondary states are sparse and $\langle\psi_p|\mathscr{H}_z|\psi_s\rangle$ is nonzero, a magnetic quenching occurs by mixing of mechanisms I and II. At lower magnetic fields, k_{mag} increases rapidly with increasing field strength. At higher fields, k_{mag} increases quadratically with magnetic field strength.

Selection Rule for Mechanism I. – The wave function of a polyatomic molecule is represented by $|\Gamma_{vibronic}\,\Gamma_\sigma\,JMNKS\rangle|R\rangle$. Here, $\Gamma_{vibronic}$ and Γ_σ are irreducible representations of a vibronic state and a spin state, respectively. J is the total angular momentum, its projection on the space-fixed z-axis being M. Coupling of orbital and rotational angular momenta results in N, its projection on the molecule-fixed z-axis being K. S is the spin angular momentum and $|R\rangle$ is a vibrational wave function. $\langle\psi_p|\mathscr{H}_z|\psi_s\rangle$ is written by the following equation:

$$\begin{aligned}\langle\psi_p|\mathscr{H}_z|\psi_s\rangle &= \langle\Gamma JMNKS|f_1(X)+gf(S)|\Gamma'J'M'N'K'S'\rangle\langle R|R'\rangle\mu_0\mathscr{H} \\ &= [\Gamma x\Gamma_R x\Gamma']\langle JMNKS|f_1(X)+gf_1(S)|J'M'N'K'S'\rangle\langle R|R'\rangle\mu_0\mathscr{H}\end{aligned} \tag{3}$$

Here, Γ_R is an irreducible representation of an axial vector, and $[\Gamma x\Gamma_R x\Gamma']$ is equal to 1 for the case where $\Gamma x\Gamma_{R_1} x\Gamma' = \Gamma_{totally\ symmetric}$ and zero for other cases. $f_1(S)$ and $f_1(X)$ are the spherical tensors of rank 1, and are the electron-spin angular momentum operator and the angular momentum operator other than the spin angular momentum, respectively.

By the use of the *Wigner-Eckart* theorem and properties of the matrix elements of a tensor operator [19], the following equations are derived.
For $\Delta K=0$ and $\Delta S=0$ transitions,

$$\begin{aligned}&\langle JMNKS|f_1(X)+gf_1(S)|J'MN'KS\rangle = (-1)^{J-M}[(2J+1)(2J'+1)]^{1/2}\begin{pmatrix} J & 1 & J' \\ -M & 0 & M\end{pmatrix} \\ &\times(-1)^{N+S+J'+1}\begin{Bmatrix} N & J & S \\ J' & N' & 1\end{Bmatrix}(-1)^{N-K}[(2N+1)(2N'+1)]^{1/2}\begin{pmatrix} N & 1 & N' \\ -K & 0 & K\end{pmatrix}\langle K|f_1(X)|K\rangle \\ &+(-1)^{N'+S+J'+1}\begin{Bmatrix} S & J & N \\ J' & S' & 1\end{Bmatrix}\langle N|N'\rangle[S(S+1)(2S+1)]^{1/2}g.\end{aligned} \tag{4}$$

When $N\neq N'$, the contribution of electron spin vanishes.
For $\Delta K=\pm1$, and $\Delta S=0$ transitions,

$$\begin{aligned}&\langle JMNKS|f_1(X)+gf_1(S)|J'MN'K\pm1S\rangle \\ &=(-1)^{J-M}[(2J+1)(2J'+1)]^{1/2}\begin{pmatrix} J & 1 & J' \\ -M & 0 & M\end{pmatrix}(-1)^{N+S+J'+1}\begin{Bmatrix} N & J & S \\ J' & N' & 1\end{Bmatrix} \\ &\times(-1)^{N-K}[(2N+1)(2N'+1)]^{1/2}\begin{pmatrix} N & 1 & N' \\ -K\mp1 & K\pm1 & \end{pmatrix}\langle K|f_1(X)|K\pm1\rangle.\end{aligned} \tag{5}$$

Consequently, we obtain the selection rule for mechanism I as follows:

1. $\Delta J = 0, \pm 1$
2. $\Delta M = 0,$
3. $\Delta N = 0, \pm 1$
4. $\Delta K = 0, \pm 1$
5. $\Delta S = 0,$
6. $\Gamma \times \Gamma_{R_1} \times \Gamma' = \Gamma_{\text{totally symmetric}}$
7. Either of the primary state or the secondary state has a magnetic moment.

For $\Delta J = 0, \Delta N = 0, \Delta K = 0, \Delta S = 0$, for example,

$$\langle JMNKS | f_1(X) + g f_1(S) | J'M'N'K'S' \rangle = \frac{[N(N+1)+J(J+1)-S(S+1)]MK}{2J(J+1)N(N+1)} \langle K | f_1(X) | K \rangle + \frac{[S(S+1)+J(J+1)-N(N+1)]gM}{2J(J+1)}$$

Magnetic Quenching of $^1A_2$ State of Carbon Disulfide. – The electronic state diagram of carbon disulfide is shown in *Figure 6*. The *Renner-Teller* effect causes the splitting of $^{1,3}\Delta_u$ states into the $^{1,3}A_2$ and $^{1,3}B_2$ states [20]. The possible interstate interactions for the carbon disulfide molecule are summarized in *Table 1*. From the table, we can see that the interactions of the $^1A_2$ state with the $^3A_2$, $^3B_2$, and $^1\Sigma_g^+$ states occur through the following terms:

$$\langle {}^1A_2 | \mathscr{H}_{so} + \mathscr{H}_{vib} | {}^3B_2 \rangle, \quad \langle {}^1A_2 | \mathscr{H}_{vib} | {}^3A_2 \rangle, \quad \langle {}^1A_2 | \mathscr{H}_{vib} | {}^1\Sigma_g^+ \rangle, \quad \langle {}^1A_2 | \mathscr{H}_{vib} | {}^1B_2 \rangle$$

$$[\langle {}^1B_2 | \mathscr{H}_{vib} | {}^3B_2 \rangle + \langle {}^1B_2 | \mathscr{H}_{so} + \mathscr{H}_{vib} | {}^3A_2 \rangle + \langle {}^1B_2 | \mathscr{H}_{vib} | {}^1\Sigma_g^+ \rangle] / [E({}^1B_2) - E({}^1A_2)].$$

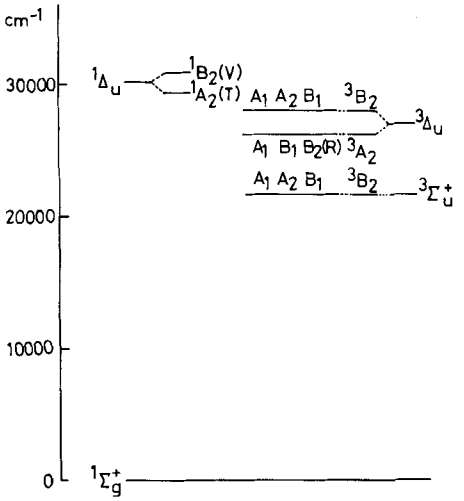

Fig. 6. *The electronic energy level diagram of carbon disulfide.* The V, T, and R systems are assigned to the $^1B_2$, $^1A_2$, and $^3A_2(B_2)$ states, respectively [20] [22]. Other electronic states are predicted theoretically [20] [21] [22] and references therein

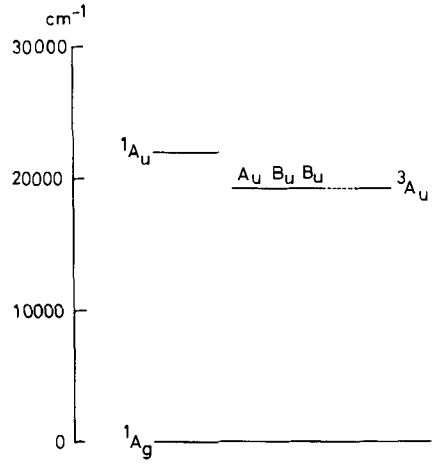

Fig. 7. *The electronic energy level diagram of glyoxal.* The absorption bands of $^1A_u \leftarrow {}^1A_g$ and $^3A_u \leftarrow {}^1A_g$ were observed by *Ramsay et al.* [29] [30]

The magnetic quenching of the $^1A_2$ state by mechanism II is due to enhancement of these interactions caused by the shift and broadening of the rovibronic levels of the $^3A_2$ and $^3B_2$ states in the presence of a magnetic field.

The magnetic quenching by mechanism I arises from the interaction terms:

$$\langle {}^1A_2|\mathscr{H}_z|{}^1\Sigma_g^+\rangle,\quad \langle {}^1A_2|\mathscr{H}_z|{}^1B_2\rangle\,[\langle {}^1B_2|\mathscr{H}_{vib}|{}^3B_2\rangle+\langle {}^1B_2|\mathscr{H}_{so}+\mathscr{H}_{vib}|{}^3A_2\rangle$$
$$+\langle {}^1B_2|\mathscr{H}_{vib}|{}^1\Sigma_g^+\rangle]/[E({}^1B_2)-E({}^1A_2)]\quad\text{and}$$
$$\langle {}^1A_2|\mathscr{H}_z|{}^1\Sigma_g^+\rangle[\langle {}^1\Sigma_g^+|\mathscr{H}_{so}+\mathscr{H}_{vib}|{}^3B_2\rangle+\langle {}^1\Sigma_g^+|\mathscr{H}_{so}+\mathscr{H}_{vib}|{}^3A_2\rangle]/[E({}^1\Sigma_g^+)-E({}^1A_2)].$$

We observed the MCD signals assigned to the $^1B_2 \leftarrow {}^1\Sigma_g^+$ and $^1A_2 \leftarrow {}^1\Sigma_g^+$ transitions [23]. Therefore, the $^1A_2$, $^1B_2$, and $^1\Sigma_g^+$ states have magnetic moments and the $\langle {}^1A_2|\mathscr{H}_z|{}^1\Sigma_g^+\rangle$ and $\langle {}^1A_2|\mathscr{H}_z|{}^1B_2\rangle$ terms do not vanish. Therefore, the magnetic quenching by mechanism I is to be expected for carbon disulfide. This agrees with the observation of the higher magnetic field component.

The magnetic moment of singlet states is generally caused by rotational [21] [24–26] and vibrational motions [27] [28], orbital angular momenta [24], and singlet-triplet interactions. *Douglas & Milton* [21] found that the *Zeeman* effect of CS_2 in $^3A_2(B_2)$ state originates from the rotational magnetic moment rather than the electron spin moment, because the effect is proportional to the total angular momentum J. This indicates that the rotational magnetic moment is important in the $^1A_2$, state, the $^1B_2$ state, and the isoenergetic rovibronic levels of $^1\Sigma_g^+$ state. The contribution of orbital angular momentum to magnetic moments may also be important, but the *Renner-Teller* effect on the $^1\Delta_u$ state reduces its contribution to some extent. The appearance of the strong perturbation due to a singlet-triplet coupling in the absorption spectrum in the corresponding energy region [20] [22] indicates that the singlet-triplet interaction contributes to some extent to the magnetic moments of these singlet states.

Magnetic Quenching of ^1A_u State in Glyoxal. – The electronic state diagram of glyoxal is shown in *Figure 7*. Interstate interactions are possible between the ^1A_u and ^3A_u states through the spin-orbit and vibronic couplings and between the ^1A_g state and the ^1A_u or ^3A_u state through the vibronic coupling. The vibronic and spin-orbit interactions between the ^1A_u and ^3A_u states are enhanced by a magnetic field through mechanism II. This is consistent with our observation that the phosphorescence from the vibrational excited ^3A_u state increases in the presence of a

Table. *Interstate interactions in carbon disulfide*

	$^1B_2$	$^1A_2$	$^3B_2$	$^3A_2$	$^1\Sigma_g^+$
$^1B_2$	x	$\mathscr{H}_z$, vib	vib	so(B_2), vib	μ_e, vib
$^1A_2$		x	so(A_2), vib	vib	$\mathscr{H}_z$, vib
$^3B_2$			x	μ_e, so, vib, $\mathscr{H}_z$	so, vib
$^3A_2$				x	so, vib

vib: vibronic coupling; so: spin-orbit interaction; $\mathscr{H}_z$: *Zeeman* interaction; μ_e: allowed electric dipole transition.

magnetic field [11]. Since the matrix element $\langle {}^1A_u|\mathscr{H}_z|{}^1A_g\rangle$ is zero, the magnetic quenching by mechanism I cannot be expected. This agrees with the experimental result that $(\tau_0/\tau)-1$ turns out to be constant at higher magnetic fields.

Magnetic Quenching of the $^3\Pi_{O_u^+}$ State in the Iodine Molecule. – Insomuch as the matrix element of $\langle {}^3\Pi_{O_u^+}|\mathscr{H}_z|{}^3\Pi_{O_u^-}\rangle$ is nonzero and the dissociative $^3\Pi_{O_u^-}$ state is a quasi-continuum, the magnetic quenching of the iodine molecule is only due to mechanism I.

Experimental Part. – Glyoxal was prepared by pyrolysis of polyglyoxal (*Wako* reagent grade) with P_2O_5.

Glyoxal molecules were excited by the use of a *Molectron* DL-200 dye (7-diethylamino-4-trifluoro-methylcoumarin) laser pumped by a *Molectron* UV-1000 nitrogen laser. The band width of the laser was 0.02 nm on tuning at 455.0 nm. Emission from gaseous glyoxal was monochromatized by a *Spex* model 1702 spectrometer and was detected by a combination of a *Hamamatsu* TV R-106 photomultiplier and a *PAR* model 160 boxcar integrator gated by a laser trigger. The photomultiplier was shielded by μ-metal in such a way that emission measurement is not affected by magnetic field. The aperture times and time bases of the boxcar integrator were 50–100 ns and 5 μs–10 μs, respectively, for the measurement of the decay time of 1–2 μs. The time-behaviour of the signal was smoothed by an RC filter with a time constant which is shorter by two orders of magnitude than the decay time to be measured.

An electromagnet with a 6.5 cm gap was used for the magnetic quenching experiments, its field strength being calibrated by a *Rowson-Lush* gaussmeter indicator Type 789. Sample pressure was measured by a MKS *Baratron* capacitance manometer consisting of a Type 310 AHS-10 head and Type 210 M-XRC indicator. A vacuum system used is free from H_g and back-ground pressure is 10^{-6} Torr.

A Pyrex-glass cross-shaped sample cell, the diameter and length of which are 6.3 cm and 10 cm, respectively, was used for the emission measurements.

REFERENCES

[1] *W. Steubing*, Verh. d. D. phys. Ges. *15*, 1181 (1913).
[2] *L.A. Turner*, Z. Physik *65*, 464 (1930).
[3] *J.H. van Vleck*, Phys. Rev. *40*, 544 (1932).
[4] *E.O. Degenkolb, J.I. Steinfeld, E. Wasserman & W. Klemperer*, J. chem. Physics *51*, 615 (1969).
[5] *W.M. Huo*, J. chem. Physics *57*, 3110 (1970).
[6] *G.A. Capelle & H.P. Broida*, J. chem. Physics *57*, 5027 (1972).
[7] *C.D. Chapman & P.R. Bunker*, J. chem. Physics *57*, 2951 (1972).
[8] *R. Solarz, S. Butler & D.H. Levy*, J. chem. Physics *58*, 5172 (1973).
[9] *S. Butler, C. Kahler & D.H. Levy*, J. chem. Physics *62*, 815 (1975).
[10] *A. Matsuzaki & S. Nagakura*, Chem. Letters *7*, 675 (1974); Bull. Chem. Soc. Japan *49*, 359 (1976).
[11] *A. Matsuzaki & S. Nagakura*, Z. physikal. Chem. (N.F.) *101*, 283 (1976).
[12] *P.W. Atkins & P.R. Stannard*, Chem. Physics Letters *47*, 113 (1977).
[13] *H.G. Küttner, H.L. Selzle & E.W. Schlag*, Chem. Physics Letters *48*, 207 (1977).
[14] *P.R. Stannard*, private communication.
[15] *A. Matsuzaki & S. Nagakura*, Proceedings of Conference 'Molecular Structure', p. 409–491, August 1977.
[16] *G.W. Robinson & C.A. Langhoff*, Chem. Physics *5*, 1 (1974).
[17] *M. Bixon & J. Jortner*, J. chem. Physics *50*, 3284 (1969).
[18] *J.C.D. Brand, J.L. Hardwick, D.R. Humphrey, Y. Hamada & A.J. Merer*, Canad. J. Physics *54*, 186 (1976).
[19] For example, *A.R. Edmonds*, 'Angular momentum in quantum mechanics', Princeton 1957.
[20] *Ch. Jungen, D.N. Malm & A.J. Merer*, Canad. J. Physics *51*, 147 (1973).
[21] *A.E. Douglas & E.R.V. Milton*, J. chem. Physics *41*, 357 (1964).
[22] *B. Kleman*, Canad. J. Physics *41*, 2034 (1963).

[23] *A. Matsuzaki & S. Nagakura*, unpublished data.
[24] *G. Herzberg*, 'Electronic Spectra of Polyatomic Molecules', van Nostrand Reinhold Company, 1966.
[25] *G.C. Wick*, Z. Physik *85*, 25 (1933).
[26] *J.R. Eshbach & M.W.P. Strandberg*, Phys. Rev. *85*, 24 (1952).
[27] *W. Hüttner & K. Morgenstern*, Z. Naturforsch. *25*, 547 (1970).
[28] *R.E. Moss & A.J. Perry*, Mol. Physics *25*, 1121 (1973).
[29] *W. Goetz, A.J. McHugh & D.A. Ramsay*, Canad. J. Physics *48*, 1 (1970).
[30] *J. Paldus & D.A. Ramsay*, Canad. J. Physics *45*, 1389 (1967).

58. Effets de l'environnement sur le couplage hyperfin du radical $Ph_2\dot{P}$

par **Théo Berclaz** et **Michel Geoffroy**

Département de Chimie Physique, Ecole de Chimie
30, quai E. Ansermet, 1211 Genève 4

(10.XI.77)

Matrix effects on the hyperfine coupling of $Ph_2\dot{P}$

Résumé

Le radical $Ph_2\dot{P}$ est piégé dans un monocristal de Ph_3PBH_3 irradié. Après élévation de température à 130 °C, ce radical se réoriente pour occuper des sites inéquivalents dans la matrice cristalline. Contrairement à la constante de couplage anisotrope, la constante de couplage hyperfin isotrope avec ^{31}P est très sensible à l'environnement du radical. Une explication est proposée pour rendre compte de cet effet de matrice.

Introduction. – L'étude par RPE. de composés paramagnétiques piégés dans des matrices cristallines constitue certainement l'une des méthodes les plus efficaces pour accéder à la structure de radicaux organiques. Ces dernières années, de très nombreuses espèces radicalaires résultant de l'action des rayons ionisants sur des substances organiques et organométalliques ont été étudiées à l'aide de cette technique [1]. Cependant, lors de telles investigations, l'influence de la matrice cristalline sur les constantes de couplage est le plus souvent négligée et nous nous proposons de mettre en évidence l'effet de ces contraintes sur la répartition du spin dans le radical diphénylphosphinyle.

Très récemment, ce radical phosphoré a été étudié dans trois matrices cristallines différentes: Ph_3P [2], Ph_3PO et $Ph_2P(S)H$ [3]. Nous donnons ici les paramètres RPE. de ce radical piégé dans un monocristal de Ph_3PBH_3 et rapportons comment, à l'intérieur du même cristal moléculaire, la réorientation de $Ph_2\dot{P}$ provoquée par une élévation de température se répercute sur la structure du radical.